Inorganic Chemistry

Article

pubs.acs.org/IC

Local and Cooperative Jahn–Teller Effect and Resultant Magnetic Properties of M_2AgF_4 (M = Na–Cs) Phases

Dominik Kurzydłowski,[*,†,‡] Tomasz Jaroń,[†] Andrew Ozarowski,[*,§] Stephen Hill,[*,§,∥] Zvonko Jagličić,[⊥] Yaroslav Filinchuk,[#] Zoran Mazej,[*,▽] and Wojciech Grochala[*,†]

[†]Centre of New Technologies, University of Warsaw, Banacha 2c, 02-097, Warsaw, Poland

[‡]Faculty of Mathematics and Natural Sciences, Cardinal Stefan Wyszynski University in Warsaw, Wóycickiego 1/3, 01-938, Warsaw, Poland

[§]National High Magnetic Field Laboratory, Florida State University, 1800 E. Paul Dirac Drive, Tallahassee, Florida 32310, United States

[∥]Department of Physics, Florida State University, Tallahassee, Florida 32306, United States

[⊥]Faculty of Civil and Geodetic Engineering, Institute of Mathematics, Physics and Mechanics, University of Ljubljana, Jadranska 19, SI-1000, Ljubljana, Slovenia

[#]Institute of Condensed Matter and Nanosciences, Université Catholique de Louvain, Place L. Pasteur, B-1348, Louvain-la-Neuve, Belgium

[▽]Department of Inorganic Chemistry and Technology, Jožef Stefan Institute, Jamova 39, SI-1000, Ljubljana, Slovenia

Supporting Information

ABSTRACT: The crystal structure, magnetic properties, heat capacity, and Raman spectra of double-perovskite M_2AgF_4 (M = K, $K_{3/4}Rb_{1/4}$, $K_{1/2}Rb_{1/2}$, $K_{1/4}Rb_{3/4}$, and Rb) phases have been examined, adding to the body of previous results for the M = Na, Cs derivatives. The results suggest that double-perovskite K_2AgF_4 adopts a disordered orthorhombic *B*mab structure with an antiferrodistortive arrangement of the elongated and tilted [AgF_6] octahedra rather than the structure with the ferrodistortive arrangement of compressed octahedra, as suggested previously (Mazej, Z.; Goreshnik, E.; Jagličić, Z.; Gaweł, B.; Łasocha, W.; Grzybowska, D.; Jaroń, T.; Kurzydłowski, D.; Malinowski, P. J.; Koźmiński, W.; Szydłowska, J.; Leszczyński, P. J.; Grochala, W. $KAgF_3$, K_2AgF_4 and $K_3Ag_2F_7$: important steps towards a layered antiferromagnetic fluoroargentate(II). *CrystEngComm* **2009**, *11*, 1702–1710). A re-examination of the previously collected single-crystal X-ray diffraction data confirms the current structure assignment, and it is also in agreement with recent theoretical calculations. High-field electron paramagnetic resonance spectra reaffirm the presence of elongated [AgF_6] octahedra in the crystal structure of all M_2AgF_4 phases studied. The local structure of the M = K derivative is most complex, with regions of the sample that are quite orthorhombically distorted, whereas other regions more closely resemble the tetragonal phase. The mixed-cation K/Rb phases are also inhomogeneous, containing regions of the pure K compound and regions of another high-symmetry phase (likely tetragonal) of a mixed (Rb-richer) compound with unknown composition. The temperature-resolved phase diagram of all K/Rb phases has been established and positioned within the entire M = Na, K, Rb, Cs series.

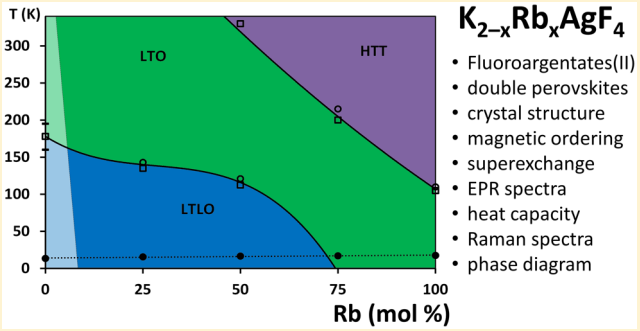

INTRODUCTION

Ternary fluorides of divalent silver have been known for more than 40 years,[1−4] yet only recently have they attracted a large amount of interest for their potential to become a new class of high-temperature superconductors (HTSCs).[5−7] These compounds, containing the Jahn–Teller (JT) active Ag^{2+} cation, were also investigated in the context of magneto-structural correlations[8−10] with the magnetic properties arising from the spin-$^1/_2$ $4d^9$ configuration of the Ag^{2+} cation. These efforts resulted in the experimental determination of a very strong antiferromagnetic interaction in $KAgF_3$,[11] similar in magnitude to that found in the oxocuprate(II) precursor of the HTSCs.

Compounds with M_2AgF_4 stoichiometry (M = Na, K, Rb, Cs) have attracted particular interest as their composition resembles that of La_2CuO_4, a prototypical precursor for oxocuprate(II) superconductors. This compound adopts the layered perovskite structure (Figure 1a)[12] and exhibits strong

Received: August 22, 2016
Published: October 18, 2016

DOI: 10.1021/acs.inorgchem.6b02037
Inorg. Chem. 2016, 55, 11479–11489

antiferromagnetic (AFM) coupling within the $[CuO_{4/2+2}]^{6-}$ layers.[13]

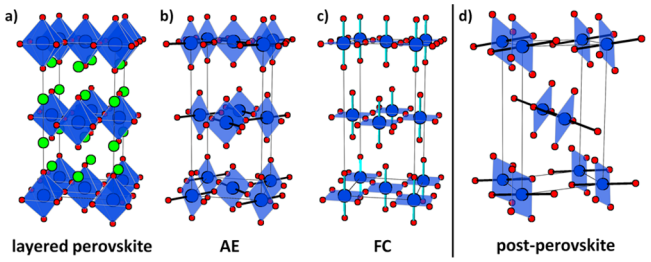

Figure 1. Layered perovskite structure type (a) together with two variants of the collective JT effect applied to this phase: AE (b) and FC (c). See the text. The postperovskite Na_2CuF_4-type structure (d) is also shown. The JT-active cations (Ag^{2+}) are marked in blue, nonmagnetic cations (K^+−Cs^+) are in green, and anions (F^-) are in red. The direction of axial elongation/compression of the $[AgF_6]^{4-}$ octahedra is marked with a black/light-blue line. For easier comparison, the nonmagnetic cations are not shown in b−d; possible titling of $[AgF_6]^{4-}$ was also omitted.

The cesium derivative of M_2AgF_4, Cs_2AgF_4, was also found to exhibit the layered-perovskite structure.[4,14,23] In this compound, the elongated $[AgF_6]^{4-}$ octahedra are arranged in an antiferrodistortive pattern within the $[AgF_{4/2+2}]^{2-}$ planes, a manifestation of the so-called collective Jahn−Teller effect.[15,16] Hereinafter we will refer to such a variant of the layered-perovskite structure as AE (antiferrodistortive/elongated, Figure 1b). The cesium derivative of M_2AgF_4 exhibits weak 2D ferromagnetic (FM) coupling with a magnetic ordering temperature (T_c) of 14 K.[17,18]

Many experimental studies[19−22] on the other members of the M_2AgF_4 series showed that these systems exhibit a high degree of structural complexity, which leads to marked differences in magnetic properties. From electron paramagnetic resonance (EPR) measurements, the structure of Rb_2AgF_4 was established to be analogous to that of Cs_2AgF_4.[23] For K_2AgF_4, two polymorphs were obtained: a metastable layered perovskite phase (α),[19] which we will term high temperature (HT), and a postperovskite Na_2CuF_4-type phase (β, low temperature − LT), which is the ground-state polymorph at room temperature.[20] It should be noted that the HT perovskite polymorph of K_2AgF_4 is kinetically stable (metastable) up to 470 K;[20] therefore, its physical properties can be characterized from low temperatures up to above room temperature.

Interestingly, HT-K_2AgF_4 was presumed to exhibit a ferrodistortive ordering of compressed octahedra within the $[AgF_{4/2+2}]^{2-}$ layers in contrast to the rubidium and cesium derivatives. The ferrodistortive variant of the layered perovskite phase, termed by us as FC (ferrodistortive/compressed), is shown in Figure 1c. Also, for the HT-K_2AgF_4 structure, tilting of the $[AgF_6]^{4-}$ octahedra was observed. Finally, for the sodium derivative, only the postperovskite Na_2CuF_4-type phase was obtained.[21] For comparison with AE and FC layered-perovskite structures, the postperovskite Na_2CuF_4-type phase, adopted by LT-K_2AgF_4 and Na_2AgF_4, is shown in Figure 1d. It is characterized by chains of edge-sharing elongated octahedra with the axes of elongation being parallel for neighboring octahedra. In other words, this structure exhibits a ferrodistortive order but is distinguished from FC by a different connectivity of the Ag/F sublattice.

The magnetic properties of both Rb_2AgF_4 and HT-K_2AgF_4 imply ferromagnetic coupling within the $[AgF_{4/2+2}]^{2-}$ planes, with ordering temperatures close to that of Cs_2AgF_4.[3,19] In the postperovskite (Na_2CuF_4-type) LT-K_2AgF_4 and Na_2AgF_4 phases, the magnetic coupling between Ag(II) centers is very weak; consequently, those compounds exhibit paramagnetic behavior even at low temperatures.[20,21]

Theoretical studies on M_2AgF_4 compounds[24−29] managed to rationalize the tendency for the adoption of the AE-type ordering in the layered perovskite phase of Cs_2AgF_4. Importantly, a recent study cast into doubt the structural assignment of the layered perovskite HT phase of K_2AgF_4.[29] These calculations showed that the experimentally derived FC-type structure has a much higher energy than a similar structure characterized by an AE-type ordering.

Here we present a reanalysis of the X-ray diffraction (XRD) data for HT-K_2AgF_4 as well as the results of high-field EPR (HFEPR) measurements, which enable an unambiguous assignment of the structure of this phase. We also perform HFEPR measurements at selected temperatures for other members of the M_2AgF_4 series (LT-K_2AgF_4, Rb_2AgF_4, and Cs_2AgF_4). From these, we deduce the structural evolution of these compounds with temperature. Finally, to better characterize the composition region at the borderline of stability of the layered perovskite phase, we synthesize new compounds with $K_{2-x}Rb_xAgF_4$ stoichiometry (x = 0.5, 1, 1.5) and conduct temperature-resolved HFEPR and XRD measurements. The obtained results enable us to fully understand and rationalize the surprising complexity of the M_2AgF_4 systems.

EXPERIMENTAL METHODS

Synthesis. Most of the studied compounds were prepared from AgF_2 and the corresponding alkali metal fluorides following procedures described previously.[19] A typical synthesis included fine powdering of the reactants in stoichiometric amounts (e.g., an KF/RbF/AgF_2 ratio of 3:1:2 for the synthesis of $K_{1.5}Rb_{0.5}AgF_4$) in an agate mortar and placing them in a Pt boat enclosed in a nickel reactor. The synthesis was conducted at 500 °C (or 300 °C in the case of LT-K_2AgF_4). The most convenient synthesis route toward high-purity samples of Na_2AgF_4 is the thermal decomposition of the $NaAgF_4$/NaF mixture under dynamic vacuum.[21] All synthesized compounds are sensitive to moisture and were handled in a glovebox operating under an argon atmosphere.

X-ray Powder Diffraction. X-ray powder diffraction (XRPD) data was collected at ambient temperature on samples placed in 0.3 mm quartz capillaries with the use of a Bruker D8 Discover diffractometer with a Cu Kα X-ray tube (λ = 1.5406 Å). The measurements were carried out in the typical range of 2θ from 10 to 120° with a 0.018° step. Cell indexing was performed with the X-Cell program embedded in the Materials Studio package (BIOVIA). Rietveld refinement was made in JANA2006.[30]

Temperature-resolved XRPD measurements were conducted on a diffractometer equipped with a rotating Mo anode (λ = 0.7093 Å) and a 2D MAR345 detector. Scans from a 0.3 mm quartz capillary filled with $K_{2-x}Rb_xAgF_4$ were collected upon heating from 80 to 330 K at 20 K/h (HT-K_2AgF_4, $KRbAgF_4$, $K_{0.5}Rb_{1.5}AgF_4$) and 40 K/h ($K_{1.5}Rb_{0.5}AgF_4$, Rb_2AgF_4) rates. The 2D images were integrated into 1D patterns with FIT2D[31] and analyzed in the FullProf suit.[32]

The obtained diffractograms indicated that all members of the $K_{2-x}Rb_xAgF_4$ series adopt the layered-perovskite structure (Figure 1a). An analysis of the systematic absences pointed to a statistical occupation of the A sites by K/Rb, i.e., no particular ordering pattern was found to prevail. During the Rietveld refinement, the relative occupancy of these sites was varied, and the resulting stoichiometry was in good accordance with that derived from the AgF_2/KF/RbF ratio used in the synthesis.

DOI: 10.1021/acs.inorgchem.6b02037
Inorg. Chem. 2016, 55, 11479−11489

Table 1. Comparison of the Structure Parameters of FC_α and AE_α^{disord} Models of HT-K_2AgF_4[a]

space group	FC_α[b]	AE_α^{disord}[c]
	Bmab[d]	
Z	4	
R_1/wR_2[e]	3.06%/7.89%	2.47%/5.91%
a (Å)	6.182(3)	6.1835(5)
b (Å)	6.436(3)	6.4372(5)
c (Å)	12.632(5)	12.634(1)
K	0.5; 0.190(2); 0.1431(1)	0.526(2); 0.0193(2); 0.1432(1)
	8f; occ 1; U_{iso} = 0.0294(4)	16g; occ 0.5; U_{iso} = 0.019(1)
Ag	0.0; 0.0; 0.0	0.0; 0.0; 0.0
	4a; occ 1; U_{iso} = 0.0138(3)	4a; occ 1; U_{iso} = 0.0134(3)
F_{ap}	0.5; 0.4301(7); 0.1611(4)	0.467(2); 0.4304(7); 0.1608(4)
	8f; occ 1; U_{iso} = 0.039(1)	16g; occ 0.5; U_{iso} = 0.020(3)
F_{eq}	0.25; 0.25; −0.0282(4)	0.253(2); 0.2895(7); −0.0284(4)
	8e; occ 1; U_{iso} = 0.057(2)	16g; occ 0.5; U_{iso} = 0.029(2)
R_{Ag-F} (Å)	F_{ap}: 2.084(6)	F_{ap}: 2.090(4)
	F_{eq}: 2.259(1)	F_{eq}: 2.07(1), 2.459(9)

[a]For each atom, the fractional (*x*, *y*, *z*) position is given along with the Wyckoff site label, the site occupancy, and the isotropic displacement factor. [b]Reference 19. [c]This work. [d]Nonstandard setting of the *Cmca* space group, which retains the *c* lattice vector as perpendicular to the $[AgF_{4/2+2}]^{2-}$ sheets. [e]$R_1 = \Sigma||F_o| - |F_c||/\ \Sigma|F_o|$ for $I > 2\sigma(I)$, $wR_2 = \Sigma|(|F_o| - |F_c|)w^{1/2}|/\ \Sigma(|F_o|w)$ for $I > 2\sigma(I)$.

Electron Paramagnetic Resonance (EPR). High-field, high-frequency EPR spectra at temperatures ranging from ca. 3 to 290 K were recorded on a home-built spectrometer at the EMR facility of the NHMFL.[33] The instrument is equipped with a superconducting magnet (Oxford Instruments) capable of reaching a field of 17 T. Microwave frequencies over the range of 52−416 GHz were generated by a phase-locked Virginia Diodes source, producing a base frequency of 13 ± 1 GHz, which was multiplied by a cascade of frequency multipliers. The instrument is a transmission-type device and uses no resonance cavity. A liquid He-cooled InSb bolometer (QMC Instruments Ltd.) was used as a microwave detector. All spectra were recorded in derivative, dI/dB (where I is the absorption intensity), mode using field modulation and a phase-sensitive lock-in detection scheme.

Because the samples are tremendously moisture-sensitive, they were packed in sample holders (φ_{in}= 7 mm, φ_{out}= 9 mm, l = 26 mm) made from perfluoropolymers and protected with two tightly fitting PTFE (Teflon) stoppers (l = 28 mm; see the SI for a photograph of a holder).

Magnetic Measurements. Magnetic measurements were performed using Quantum Design MPMS-XL-5 SQUID and MPMS SQUID VSM magnetometers. The temperature dependence of the susceptibility was measured between 2 and 300 K in a magnetic field of 1 kOe. The obtained data has been corrected for the contribution of an empty sample holder (quartz/FEP for XL-5/VSM) as well as for then temperature-independent diamagnetism of inner shell electrons.[34]

RESULTS AND DISCUSSION

Jahn−Teller Ordering in HT-K_2AgF_4. Because the X-ray scattering factor of fluorine is more than 5 times smaller than that of silver X-ray diffraction (XRD), investigations yield information only on the approximate position of fluorine atoms. Furthermore, in the case of the layered perovskite M_2AgF_4 phases, different competing JT orders are possible (Figure 1). Consequently, we found that the XRD technique is insufficient for the unambiguous determination of the JT order present in the layered perovskite phases of M_2AgF_4 compounds (in particular, Rb_2AgF_4; see the Supporting Information, section I).

In the previous single-crystal X-ray diffraction study conducted at 200 K, the crystal structure of HT-K_2AgF_4 was assigned to the FC_α structure.[19] The α subscript indicates the type of tilting distortion present in this structure; for details, see ref 29. Theoretical calculations show that the FC_α structure has a much higher energy (over 0.15 eV per K_2AgF_4 unit) than the AE_α arrangement (i.e., the AE-type structure with the same tilting distortions as for the FC_α).[29]

We therefore reanalyzed the single-crystal data by performing a refinement on the AE_α model. To our surprise, this did not lead to a significant improvement in the goodness-of-fit parameters. We then turned to a structure that, similar to AE_α, contained antiferrodistortive JT order and α-type tilts but additionally exhibited disorder in the orientation of neighboring octahedra. This structure, which we term AE_α^{disord}, exhibits the same symmetry as FC_α. It turned out to give a much better fit to X-ray data than FC_α (Table 1). For more details concerning AE_α^{disord}, see the cif file in the SI. This structure is also deposited in the ICSD database under the number 431905.

From the above, we can conclude that indeed HT-K_2AgF_4 exhibits AE-type Jahn−Teller ordering, similar to that in Rb_2AgF_4 and Cs_2AgF_4 and in accordance with DFT + U calculations.[29] To further confirm this result, we turned to a complementary nondiffraction technique that can provide information on the Jahn−Teller distortion by conducting high-field electron paramagnetic resonance (HFEPR) measurements for all members of the M_2AgF_4 family that exhibit the layered perovskite structure (Cs_2AgF_4, Rb_2AgF_4, HT-K_2AgF_4, as well as mixed K/Rb compounds described further below). As can be seen in Figure 2, all three pure compounds exhibit very similar axial spectra, with just two *g*-tensor components: the measured perpendicular and parallel values are approximately 2.25(g^{ex}_{xy}) and 2.07(g^{ex}_{z}), respectively. The resonance fields were determined at various microwave frequencies from 24 to 406 GHz and at 200 K to avoid complications associated with magnetic ordering (see below). The extrapolated plots of the resonance fields versus frequency pass through the origin (B = 0, ν = 0), meaning that the equation $h\nu = g\mu_B B$ is obeyed, there is no zero-field splitting of the levels involved in the EPR transitions, and no measurable internal magnetic field is present (SI, Section II).

The relative magnitudes of the *g*-tensor components seem to indicate at first glance the presence of the compressed form of

DOI: 10.1021/acs.inorgchem.6b02037
Inorg. Chem. 2016, 55, 11479−11489

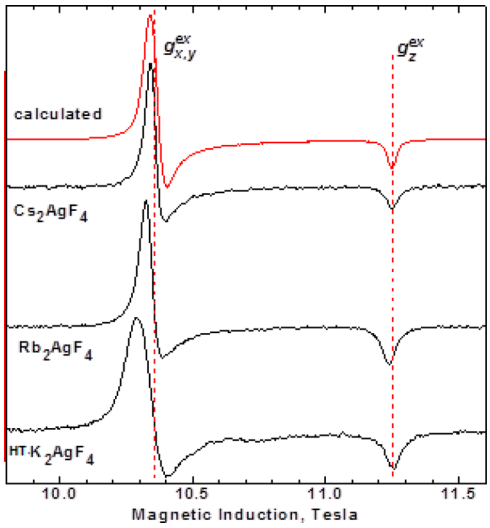

Figure 2. Powder HFEPR spectra (ν = 326.4 GHz) of HT-K_2AgF_4, Rb_2AgF_4, and Cs_2AgF_4 at 200 K. Dashed lines indicate the positions of the experimentally observed g-tensor components, g^{ex}_i (i = x, y, z), for Cs_2AgF_4. The red spectrum is the best simulation of the Cs_2AgF_4 data (see the text for an explanation).

the $[AgF_6]^{4-}$ octahedra because $g^{ex}_{xy} > g^{ex}_z$ (Table 2). However, this cannot be the case for such a geometry because g_z should be exactly equal to g_0 (= 2.0023); therefore, the corresponding resonance in Figure 2 should occur at a higher field of ca. 11.65 T. It is thus apparent that the g^{ex} values seen in the experimental spectra are not due to the isolated molecules. In fact, the spectra of all three compounds can be explained by the combined influences of the AE orbital ordering and exchange averaging (hence the "ex" superscript on the experimental g values), similar to what has previously been found for K_2CuF_4.[35]

Table 2. Intrinsic g-Tensor Components Expected for Ag^{2+} in a JT Compressed Octahedral Geometry, for Which the Unpaired Electron Resides in the dz^2 Orbital, and in a JT Elongated Geometry, with the Unpaired Electron in the $dx^2 - y^2$ Orbital[a]

	JT compressed	JT elongated
g_x	$2.0023 - \{6\lambda/[\Delta E(z^2, yz)]\}$	$2.0023 - \{2\lambda/[\Delta E(x^2 - y^2, yz)]\}$
g_y	$2.0023 - \{6\lambda/[\Delta E(z^2, xz)]\}$	$2.0023 - \{2\lambda/[\Delta E(x^2 - y^2, xz)]\}$
g_z	2.0023	$2.0023 - \{8\lambda/[\Delta E(x^2 - y^2, xy)]\}$

[a]The spin–orbit coupling constant λ for Ag^{2+} equals -1844 cm^{-1} but may be reduced due to covalence. Thus, $g_{xy} > g_z$ for the compressed case and $g_z > g_{xy}$ for the elongated case.

At 200 K, the M = Cs and Rb compounds adopt AE structures that are tetragonal (b/a = 1.00 to within the experimental accuracy, see SI Section III and ref 15), with no discernible tilting of the $[AgF_6]^{4-}$ octahedra out of the layers. Consequently, the JT elongation axis (local z) of a given ion will be parallel to one of the short axes (local x) of its four nearest neighbors within the same plane, whereas the other short axes of the neighbors (local y) are oriented perpendicular to the plane (Figure 1b). For this high-symmetry case, the intrinsic Ag(II) g-tensor components (g_x, g_y, g_z) combine according to eqs 1 and 2 to give an exchange-averaged effective g tensor that is tetragonal, in accordance with the experimental observations:

$$g^{ex}_z = g_y \tag{1}$$

$$g^{ex}_{xy} = \frac{1}{2}(g_x + g_z) \tag{2}$$

Equation 2 implies an exact perpendicular arrangement of the Z axes of the interacting ions. With an angle of $\alpha \neq 90°$ between the Z axes of interacting ions, eq 2 can be generalized as follows:

$$g^{ex}_x = \frac{g_x + g_z + (g_z - g_x)\cos\alpha}{2} \tag{2a}$$

$$g^{ex}_y = \frac{g_x + g_z - (g_z - g_x)\cos\alpha}{2} \tag{2b}$$

Nonaxial EPR spectra are thus expected for $\alpha \neq 90°$. Two different perpendicular g components should be seen as a result of the tilting.

If one then assumes local g tensors corresponding to the JT elongated case in Table 2 (i.e., $g_x = g_y$ and $g_z > g_{xy}$), then the intrinsic g-tensor components can be extracted from the exchange-averaged ones in Figure 2, giving g_{xy} = ca. 2.07 and g_z = ca. 2.44. These values are in excellent agreement with those previously determined at 130 K for Cs_2AgF_4 (g_z = 2.07, g_{xy} = 2.42) and Rb_2AgF_4 (g_z = 2.07, g_{xy} = 2.43)[23] and postperovskite LT-K_2AgF_4 (g_z = 2.42, g_{xy} = 2.10) at 150 K.[20] In this work, values of g_z = 2.427, g_y = 2.100, and g_x = 2.077 were determined at 200 K for LT-K_2AgF_4 (Table 3). This suggests that very similar coordination spheres of Ag^{2+} exist in both HT and LT phases of K_2AgF_4.

The exchange-averaging phenomenon may be further understood by modeling the system as a simple dimer composed of two exchange-coupled, octahedrally coordinated Ag(II) centers, with long and short Ag···F bonds oriented in a way that mimics the actual structure. This dimer unit corresponds to the elementary building block within the 2D layers, and although its spatial symmetry is low, the symmetry of the corresponding spin Hamiltonian is tetragonal,

$$\hat{H} = \mu_B \vec{B}\cdot\vec{\vec{g}}_1\cdot\hat{s}_1 + \mu_B \vec{B}\cdot\vec{\vec{g}}_2\cdot\hat{s}_2 - J\hat{s}_1\cdot\hat{s}_2 \tag{3}$$

where $\hat{s}_j$ and $\vec{\vec{g}}_j$ (j = 1, 2) correspond respectively to the local spin operators and intrinsic g tensors at the two sites within the

Table 3. Diagonal g^{ex}-Tensor Components Determined Experimentally at 200 K for the Layered-Perovskite Structures

	LT-K_2AgF_4[a]	HT-K_2AgF_4	$K_{1.5}Rb_{0.5}AgF_4$	$KRbAgF_4$	$K_{0.5}Rb_{1.5}AgF_4$	Rb_2AgF_4	Cs_2AgF_4
g^{ex}_x	2.077	2.259	2.260	2.258	2.259	2.255	2.252
g^{ex}_y	2.100	2.259	2.260	2.258	2.259	2.255	2.252
g^{ex}_z	2.427	2.072	2.075	2.076	2.075	2.075	2.073

[a]LT-K_2AgF_4 exhibits ferrodistortive order (Figure 1d), and g^{ex} components reflective of the intrinsic values are directly observed. All of the others are AE (or AE_α^{disord}) ordered, and axial exchange-coupled g^{ex} values are given.

DOI: 10.1021/acs.inorgchem.6b02037
Inorg. Chem. 2016, 55, 11479–11489

dimer, and J is the exchange coupling strength. The structure then dictates that $g_{1x} = g_{2y} = 2.44$, $g_{1y} = g_{2x} = 2.07$, and $g_{1z} = g_{2z} = 2.07$, where the coordinates are now referenced to the dimer frame (i.e., x and y correspond to the JT elongation axes on sites 1 and 2, respectively, and z represents the normal to the layers). Taking the experimental value of $J = 30$ cm^{-1} for Cs_2AgF_4,[15] an axial ($g^{ex}_x = g^{ex}_y$) simulated spectrum is obtained, in accord with the experimental results (see Figure 2, top).

The HT-K_2AgF_4 compound, meanwhile, adopts the distinctly orthorhombic AE_α^{disord} structure ($b/a \approx 1.04$ at 200 K, see the SI, Section III) with accompanying tilting of the $[AgF_6]^{4-}$ units about (100). This should give rise to a nonaxial exchange-averaged g tensor (i.e., g^{ex}_x should be different from g^{ex}_y). According to eqs 2a and 2b, these g^{ex}_x and g^{ex}_y values should be centered on the $g^{ex}_{xy} = (g_x + g_z)/2 = 2.26$ value, which is observed at 200 K for all samples (Figure 2). The degree of splitting will depend on the precise details of the local coordination at different Ag(II) sites in the lattice, which is not well established from XRD studies. Meanwhile, the disorder associated with the AE_α^{disord} structure will likely further complicate matters, as some regions of the crystal are more orthorhombic than others. Consequently, a continuous distribution of g^{ex}_x and g^{ex}_y values may be expected, centered on 2.26, thus explaining the single broad g^{ex}_{xy} component observed for the HT-K_2AgF_4 compound at high temperatures. The fact that this resonance is substantially broader than all other features in Figure 2 seems to support this hypothesis, which is further confirmed by the low-temperature spectra (see below).

Therefore, on the basis of the analysis of HFEPR data we have concluded that the HT-K_2AgF_4 polymorph exhibits a layered perovskite structure with an antiferrodistortive ordering of elongated octahedra analogous to that found in Cs_2AgF_4. The only difference between Cs_2AgF_4 and HT-K_2AgF_4 would be the disorder and presence of tilting distortions in the latter. This is further supported by the striking similarities in the Raman spectra of HT-K_2AgF_4/Rb_2AgF_4 and Cs_2AgF_4 (SI, Section V). This finding, which reconciles the available experimental and theoretical results, should be confirmed in the future with the neutron diffraction measurements.

Table 3 collects values of the diagonal components of the g^{ex} tensors determined at 200 K by HFEPR for layered perovskite structures in the M_2AgF_4 family (M = K, Rb, Cs), also including the mixed K/Rb phases (cf. next section). With the exception of LT-K_2AgF_4, all of the tensors are axial/tetragonal, with $g^{ex}_x = g^{ex}_y > g^{ex}_z$, reflecting the AE structures. Meanwhile, LT-K_2AgF_4 possesses a postperovskite structure with chains of ferrodistortively ordered octahedra (Figure 1d). Therefore, the experimental g-tensor components correspond exactly to the intrinsic axially JT elongated values in Table 2, with a slight distortion of the $[AgF_6]^{4-}$ octahedra giving rise to a rhombic g-tensor with $g^{ex}_x \neq g^{ex}_y$.

Tilting Distortions and the Phase Diagram of the $K_{2-x}Rb_xAgF_4$ System. Having established the structural characteristics of HT-K_2AgF_4, we decided to explore the nature of the tilting distortions in the layered-perovskite $K_{2-x}Rb_xAgF_4$ systems. We synthesized three new compounds exhibiting x equal to 0.5, 1, and 1.5, which correspond to 25, 50, and 75 Rb mol %. As described in the Experimental Methods section, the room-temperature XRPD data of these compounds indicated that they adopt the layered-perovskite A_2BX_4 structure with K^+ and Rb^+ cations randomly distributed over the A sites.

We followed the changes in the lattice parameters of the mixed-cation compounds as well as those of HT-K_2AgF_4 and Rb_2AgF_4, by performing XRD measurements in the temperature range from 80 to 340 K (we found that above 340 K the studied compounds reacted with the walls of the quartz capillaries). Note that although HT-K_2AgF_4 is a metastable phase its transition to the ground-state LT-K_2AgF_4 polymorph is kinetically hindered and requires temperatures in excess of 470 K.[20]

In the studied temperature–composition range, we found evidence for three types of phases. In the investigated temperature window, all three of them are observed for $KRbAgF_4$ (Figures 3 and 4). At 80 K, this compound is

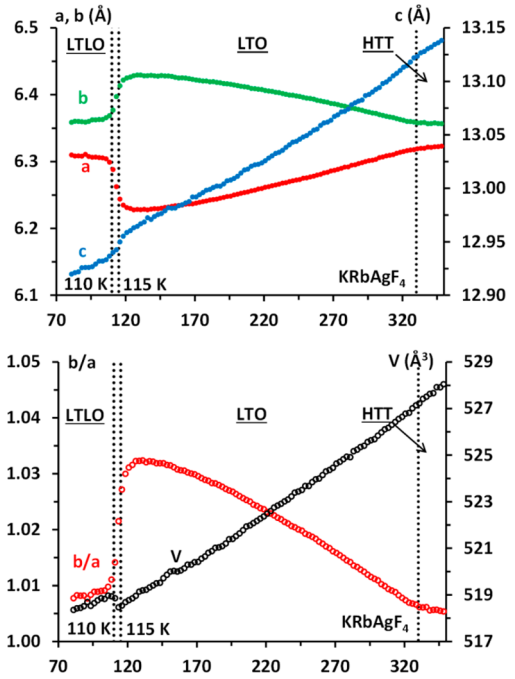

Figure 3. Temperature dependence of the lattice vectors (upper panel) as well as the volume and b/a ratio (lower panel) of $KRbAgF_4$. Dotted lines mark the boundaries between the LTLO and LTO phases (110–115 K) as well as between the LTO and HTT phases (330 K).

characterized by an orthorhombic cell with very similar lengths of the a and b lattice vectors (b/a ratio of approximately 1.01). We will refer to this phase as LTLO (low-temperature less orthorhombic). Upon heating, the b/a ratio remains nearly constant up to 110 K. Above this temperature, a drastic increase in the b/a ratio is seen (up to approximately 1.03). This marks the entrance into the LTO phase (low-temperature orthorhombic). This transition is accompanied by a volume discontinuity suggesting that it is a first-order transition.

Upon further heating, the b/a ratio of LTO decreases down to a value of 1.005 at 330 K and remains nearly constant above this temperature. At this point, the measured difference between a and b is below the resolution of the XRPD measurements, and thus we conclude that, above 330 K, the cell is tetragonal ($a = b$). Therefore, at this temperature we observe the transition into the high-temperature tetragonal phase (HTT). The LTO-HTT transition seems to be continuous with no volume discontinuity and only a slight change in the slope of the c vs T dependence.

DOI: 10.1021/acs.inorgchem.6b02037
Inorg. Chem. 2016, 55, 11479–11489

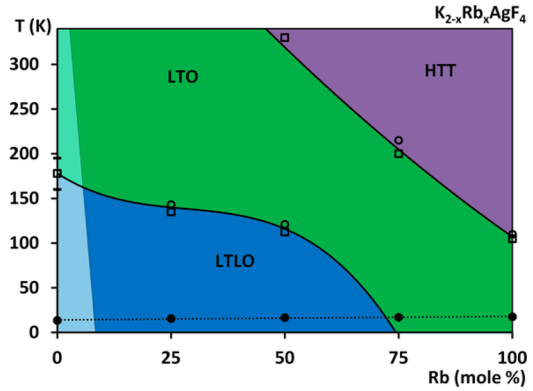

Figure 4. Phase diagram of the layered-perovskite phases of the $K_{2-x}Rb_xAgF_4$ system. Violet/green/blue colors indicate proposed regions of stability of the HTT/LTO/LTLO layered-perovskite phases. Light colors indicate the region in which the layered perovskite phase is metastable with respect to the postperovskite Na_2CuF_4-type phase adopted by LT-K_2AgF_4. Open circles/squares mark temperatures of structural transition obtained from heat capacity/XRD measurements. Filled circles mark the temperatures of the FM ordering observed in the perovskite phases.

Measurements of compounds with lower Rb content (HT-K_2AgF_4, $K_{1.5}Rb_{0.5}AgF_4$ – see SI, Section III) revealed the presence of only the LTLO-LTO transition in the studied temperature range, which appears with decreasing Rb content at progressively higher temperature and with greater hysteresis. For systems with high Rb content ($K_{0.5}Rb_{1.5}AgF_4$; Rb_2AgF_4) we observed by XRPD only the LTO-HTT transition (SI, Section III). The temperature of this transition decreases with increasing Rb content. Heat capacity measurements conducted in the 2–300 K temperature range (SI, Section IV) did not indicate any additional structural phase transitions apart from those observed by XRPD. The temperature dependence of the magnetic susceptibility (Figure 5) suggests that all perovskite $K_{2-x}Rb_xAgF_4$ phases exhibit paramagnetic behavior above 20 K, consistent with a model for a 2D spin-$^1/_2$ system[36] and 2D FM properties below ~20 K with ordering temperatures increasing slightly from K_2AgF_4 (13.4 K) to Rb_2AgF_4 (17.5 K). We have not found any evidence for anomalous behavior of the magnetic susceptibility in the vicinity of the structural phase transitions. On the other hand, the HFEPR spectra of the three phases differ significantly, as discussed in the next section (SI, Section VI).

HFEPR Studies of the Magnetic Ordering. As a microscopic probe, HFEPR can provide important information concerning the magnetic ordering in the M_2AgF_4 family, which in turn can give further insights into the low-temperature structures. It is most straightforward to first consider the simplest M = Cs and Rb cases, particularly the former as it maintains a tetragonal structure (HTT) all the way down to 5 K.[15] As seen in Figure 6, Cs_2AgF_4 displays axial spectra both at high (200 K) and low (3 K) temperatures, with just two resonances corresponding to parallel ($//z$) and perpendicular ($//xy$) mode excitations. However, the anisotropy, as measured by the spacing between these two resonances, is significantly stronger (by approximately a factor of 2 at 326 GHz) at low temperature.

From measurements performed at multiple frequencies (Figure 6, main panel), we ascertain that the additional contribution to the low-temperature anisotropy is due primarily to a field-independent interaction. In other words, the field-dependent Zeeman interaction is more or less unchanged between 200 and 3 K, with very similar g factors deduced from the slopes of linear fits to the data in Figure 6 (see also Tables 3 and 4). Note that the g_x value for HT-K_2AgF_4 does change from 2.26 at 200 K to 2.30 at 3 K but remains unchanged in the compounds containing Rb and Cs.

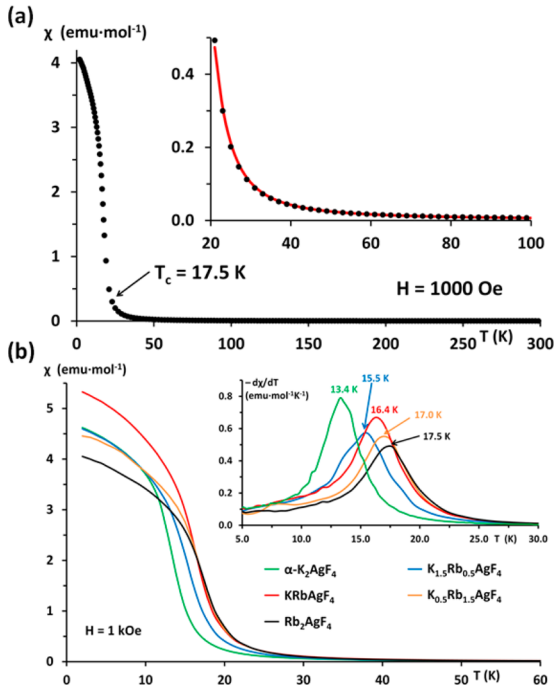

Figure 5. (a) Temperature dependence of the magnetic susceptibility of Rb_2AgF_4. The transition to the ferromagnetic state is seen at 17.5 K. The inset shows a fit in the paramagnetic region to a 2D model for a spin-$^1/_2$ system,[36] yielding g = 2.03 and J_{2D} = 4.8 meV. (b) Temperature dependence of the magnetic susceptibility of HT-K_2AgF_4, Rb_2AgF_4, and $K_{2-x}Rb_xAgF_4$. The inset shows the temperature dependence of $-d\chi/dT$ used to establish the magnetic transition temperatures.

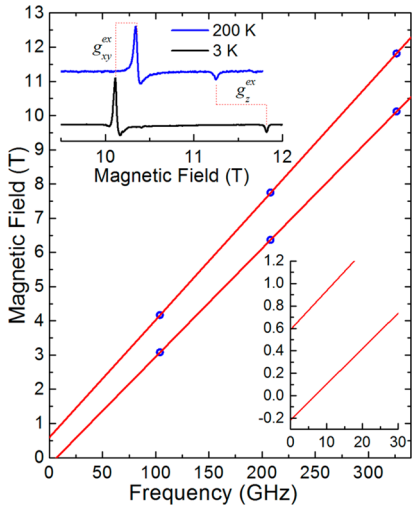

Figure 6. Frequency dependencies of the parallel (z) and perpendicular (xy) components of the EPR spectra measured for Cs_2AgF_4 at 3 K; g^{ex}_{xy} = 2.257 and g^{ex}_{z} = 2.077 are calculated from the slopes of the straight lines. The upper inset shows 326.4 GHz spectra at 200 and 3 K.

DOI: 10.1021/acs.inorgchem.6b02037
Inorg. Chem. 2016, 55, 11479–11489

Table 4. Diagonal g^{ex}-Tensor Components and Anisotropy (A) Fields Determined Experimentally at 3 K for the Layered-Perovskite Structures

	LT-K_2AgF_4[a]	HT-K_2AgF_4	$K_{1.5}Rb_{0.5}AgF_4$	$KRbAgF_4$	$K_{0.5}Rb_{1.5}AgF_4$	Rb_2AgF_4	Cs_2AgF_4
g^{ex}_x	2.067	2.303	2.254	2.270	2.268	2.26	2.257
g^{ex}_y	2.093	2.22[b]	2.254	2.270	2.268	2.26	2.257
g^{ex}_z	2.431	2.075	2.077	2.076	2.077	2.076	2.077
$B^{int}_{A\parallel}$		0.45 T	0.50 T	0.52 T	0.54 T	0.58 T	0.53 T
$B^{int}_{A\perp}$		0.35 T[d]	0	0	0.11 T	0.09 T	0
			0.35 T[c]	0.35 T[c]	0[c]	0[c]	

[a]LT-K_2AgF_4 exhibits ferrodistortive order (Figure 1d), and g^{ex} components reflective of the intrinsic values are directly observed. All others are AE (or AE_α^{disord}) ordered, and axial exchange-coupled g^{ex} values are given. [b]Estimated; see the ext. [c]Values associated with minor species. [d]The maximum value associated with a broad distribution.

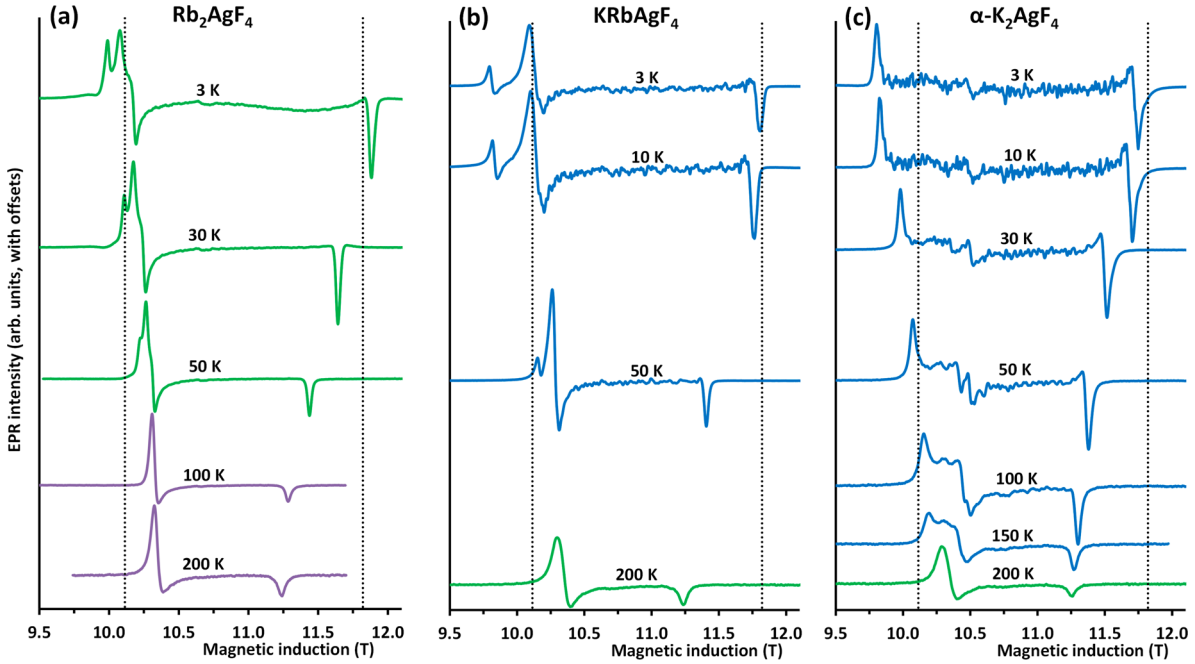

Figure 7. Powder HFEPR spectra (ν = 326.4 GHz) of Rb_2AgF_4 (a), $KRbAgF_4$ (b), and HT-K_2AgF_4 (c) at selected temperatures. Dashed lines indicate the positions of the experimentally observed g-tensor components for Cs_2AgF_4 at 3 K. Violet/green/blue mark spectra taken at temperatures where the respective compounds adopt the HTT/LTO/LTLO structure. (See the text.)

Field-independent magnetic anisotropy can have several sources.[37] At the single-site level, spin−orbit coupling gives rise to so-called zero-field-splitting interactions, although only for spin $s > {}^1/_2$.[38] Meanwhile, both short- and long-range intersite magnetic interactions can be modeled in terms of an anisotropy field, B^{int}_A, internal to the sample. Indeed, such effects may be strong in ferromagnetically ordered materials.[39] For an ordered uniaxial crystal, assuming only second-order contributions to the magnetic anisotropy, this gives rise to modified ferromagnetic resonance (FMR) conditions for fields applied parallel and perpendicular to the tetragonal axis.[37]

$$\text{parallel: } h\nu = g_z\mu_B(B + B^{int}_{A\parallel}) \quad (4)$$

$$\text{perpendicular: } h\nu = g_{xy}\mu_B\left(B - \frac{1}{2}B^{int}_{A\parallel}\right) \quad (5)$$

Here, $B^{int}_{A\parallel}$ refers to the unaxial component of the anisotropy field so as to distinguish it from the perpendicular component, $B^{int}_{A\perp}$, appropriate to the rhombic cases discussed further below. B represents the local magnetic induction, which may include an isotropic internal contribution, B^{int}_{iso}, such that $B = B^{ext} + B^{int}_{iso}$, where B^{ext} is the externally applied magnetic field. The above expressions assume $B^{int}_{A\parallel}$ to be constant (i.e., that the sample magnetization is saturated), requiring $B^{ext} > B^{int}_{A\parallel}$. An examination of the zero-frequency intercepts in Figure 6 (see inset) reveal values of +0.59 T and −0.21 T for the parallel and perpendicular modes, respectively. These are not so far from being in the 2:−1 ratio predicted on the basis of eqs 4 and 5, suggesting that B^{int}_{iso} is relatively weak in comparison to $B^{int}_{A\parallel}$. Taking the difference of these two intercepts and dividing by ${}^3/_2$ gives a value of $|B^{int}_{A\parallel}| \approx 0.53$ T, from which one can deduce that $B^{int}_{iso} \approx 0.06$ T. In fact, the signs of the intercepts dictate a negative value of $B^{int}_{A\parallel}$, indicating an easy-plane character to the field-independent anisotropy (easy xy plane and hard z axis) (i.e., the same symmetry as the field-dependent spin−orbit anisotropy) as measured by the exchange-averaged g tensor ($g_{xy} > g_z$, see Table 3).

The anisotropy field B^{int}_A can have contributions from[37] (i) dipole−dipole interactions, (ii) macroscopic demagnetizing fields, and (iii) spin−orbit-mediated exchange processes. The first two contributions to B^{int}_A would not be expected to exceed $\mu_o M^{sat}$, where M^{sat} is the saturation magnetization, with an upper bound of ∼0.1 T for the M_2AgF_4 family determined on the basis of the known structures and unit cell parameters (SI,

DOI: 10.1021/acs.inorgchem.6b02037
Inorg. Chem. 2016, 55, 11479−11489

Section VI). In fact, for the employed powder samples, one would not anticipate any appreciable magnetic anisotropy arising from demagnetizing fields because the crystallites in the powder are, on average, spherical and the sample itself has an aspect ratio that gives a demagnetizing factor similar to that of a sphere. Spherical geometry makes only an isotropic contribution to the internal field of $6B_{iso}^{int} = \frac{2}{3}\mu_0 M$, suggesting a value of about 0.07 T at saturation, which is remarkably close to the estimate above. We thus conclude that the overwhelming contribution to $B_{A\|}^{int}$ must be due to spin−orbit-mediated anisotropic exchange processes between Ag(II) sites, giving rise to a non-Heisenberg exchange Hamiltonian, $\hat{H}_{ij} = \hat{s}_i \cdot \overleftrightarrow{J}_{ij} \cdot \hat{s}_j$, where the interaction $\overleftrightarrow{J}_{ij}$ is now a tensor. The details of this physics are beyond the scope of this article, and the reader is instead referred to refs 37, 39, and 40 for an in-depth discussion.

Only the anisotropic part of this interaction influences the FMR mode frequency, thus contributing to shifts in the spectral peak positions. However, these shifts vanish at elevated temperatures because thermal fluctuations suppress local spin−spin correlations (i.e., $\langle \hat{s}_i \cdot \hat{s}_j \rangle \rightarrow 0$ or, more precisely, $\langle \hat{s}_i^{\eta} \cdot \hat{s}_j^{\eta} \rangle \rightarrow 0$, with $\eta = x, y, z$). In this sense, B_A^{int} really looks like an internal field because it emerges as the ordered ferromagnetic moment appears. One expects stronger relativistic spin−orbit effects in Ag(II) compounds than in Cu(II) compounds, and it is notable that an anisotropy field of ∼0.2 T has previously been estimated from powder EPR studies in the ordered state of AE K_2CuF_4.[23,35] It is therefore likely that these anisotropies have the same origin, with the heavier Ag(II) ions manifesting stronger spin−orbit coupling $|B_{A\|}^{int}| = 0.53$ T.

We next turn to the M = Rb compound that has a tetragonal (HTT) structure at room temperature but transitions to an orthorhombic (LTO) structure at ∼105 K (Figure 4). This is clearly borne out by the HFEPR spectra in Figure 7a. At 100 K and above, an axial spectrum is observed, with just two peaks corresponding to parallel (//z) and perpendicular (//xy) mode excitations, having g values essentially identical to those of the M = Cs compound (Table 3 and Figure 8a). However, below 100 K, the perpendicular part of the spectrum starts to exhibit fine structure indicative of a breaking of the tetragonal (i.e., $x \equiv y$) symmetry. The only complication is that three perpendicular features are observed at low temperatures.

For a small rhombic magnetic anisotropy, one would expect the B//xy portion of the spectrum to split into two components positioned symmetrically about the location of the axial xy resonance: the lower-field component should appear as a peak, with the higher-field component having a derivative shape (crossing through the spectral baseline). A comparison between the 3 K spectra for M = Cs and Rb in Figure 8b shows that this is indeed the case (i.e., that the low-field (x-field) and high-field (y-field) components of the M = Rb perpendicular spectrum are located symmetrically about the single xy resonance for the M = Cs compound. However, there is also a peak in the middle, suggesting perhaps that the LTO phase is inhomogeneous, with some regions remaining in the HTT phase or transitioning to the LTLO phase. The g values determined from the frequency dependencies of these perpendicular features are all the same (2.27) and are very close to the magnitude of g for the single perpendicular resonance observed at 200 K (2.26). This is a common characteristic of all samples except for HT-K_2AgF_4 (Figure S2). Note that when the internal field disappears at higher temperatures all of these perpendicular features will collapse into one.

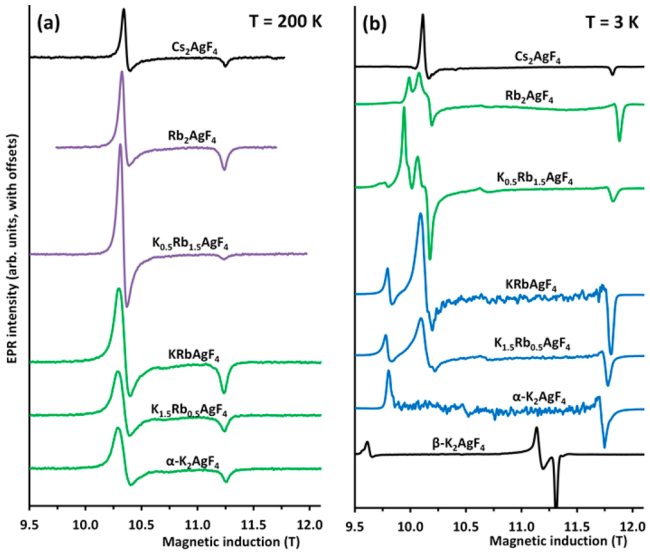

Figure 8. Powder HFEPR spectra (ν = 326.4 GHz) of the Cs_2AgF_4 and $K_{2-x}Rb_xAgF_4$ phases at 200 (a) and 3 K (b). In the case of $K_{2-x}Rb_xAgF_4$, violet/green/blue mark spectra taken at temperatures where the respective compounds adopt the HTT/LTO/LTLO structure. (See the text.) Note that because of the ferrodistortive order in the postperovskite LT-K_2AgF_4 phase the intrinsic g values are observed for this compound. The intensities of the spectra are not normalized.

The temperature dependence of the M = Rb spectra in Figure 7a (and indeed those of the mixed K/Rb compounds, Figure 7 and SI, Section VI) reveals the onset of the internal anisotropy field, B_A^{int}, at temperatures of as high as 100 K, as seen from the shifts in the z and xy components from their 200 K positions. At first glance, this seems to contradict the magnetic measurements that indicate FM ordering at ∼20 K in all compounds. However, the HFEPR studies are necessarily carried out under a large applied magnetic field (∼10−11 T), which leads to the onset of an ordered moment at a significantly higher temperature. Moreover, EPR probes magnetic correlations on rather short time scales ($\sim 1/\nu$). Thus, signatures of the ferromagnetic state (i.e., $\langle \hat{s}_i \cdot \hat{s}_j \rangle > 0$) emerge on short length/time scales well above the thermodynamic ordering temperature.[37]

As can be seen in Figure 8b, the axial component of the anisotropy field, $B_{A\|}^{int}$, as determined by the separation between the parallel resonance and the center-of-mass of the perpendicular modes at 3 K is essentially the same for the M = Cs and Rb compounds. Moreover, as we argue below, it is essentially the same for all of the studied compounds (Figure 8b and Table 4). The differences are to be found in the perpendicular components of the low-temperature EPR spectra, where splittings of the x and y resonances signify the onset of a perpendicular anisotropy field, $B_{A\perp}^{int}$, for the orthorhombic phases. The saturation values of $B_{A\perp}^{int}$ are determined at 3 K (Table 4) by the shifts of the x and y resonances from the center of the perpendicular spectrum: the y resonance shifts by $+B_{A\perp}^{int}$ and the x resonance shifts by $-B_{A\perp}^{int}$ so that the separation of the x and y components is equal to $2B_{A\perp}^{int}$. Mixed $K_{0.5}Rb_{1.5}AgF_4$ (SI, Section VI) exhibits essentially identical behavior to the all-Rb compound, although there is a hint that the onset of rhombic behavior occurs at a higher temperature,

DOI: 10.1021/acs.inorgchem.6b02037
Inorg. Chem. 2016, 55, 11479−11489

as expected on the basis of the XRPD studies (Figure 4) and that $B_{A\perp}^{int}$ increases slightly (Table 4); the central perpendicular resonance is also weaker in comparison to the rhombic ones, suggesting reduced amounts of the tetragonal phase, and there is also a hint of an additional peak at ∼9.8 T that we explain further below.

We conclude by considering the remaining $K_{2-x}Rb_xAgF_4$ compounds ($x \leq 1$) together with the pure HT-K_2AgF_4 system. As noted already, although they all start out in the LTO phase at 200 K, the rhombic anisotropy cannot be resolved in the high-temperature spectra. At low temperature, meanwhile, all of the $x \leq 1$ compounds transition to the LTLO phase. However, at first glance, the 3 K spectra appear to be more rhombic than those of the $x > 1$ compounds (Figures 7 and 8 and SI, Section VI), with a pair of well-separated low-field resonances. However, the clearest clue to what is likely happening can be seen upon comparing spectra for the mixed K/Rb and pure HT-K compounds in Figure 8b. We believe that the mixed phases are again inhomogeneous, containing regions of the pure K compound and regions of another high-symmetry phase (likely tetragonal) of a mixed (Rb-richer) compound with unknown composition. Thus, the 9.8 T perpendicular resonance is due to the pure K compound, whereas the resonance occurring at 10.1 T is due to the high-symmetry (LTLO) mixed phase. Although appreciably broader, one sees that this latter resonance has the same shape and is located at exactly the same position as the M = Cs perpendicular mode, suggesting that this phase could be very close to tetragonal, with approximately the same axial anisotropy field (Table 4). Moreover, one can clearly observe that the intensity of the peak ascribed to K, relative to the one due to the mixed K/Rb phase, decreases with decreasing K concentration, being barely discernible in the x = 1.5 compound. From Table 4, one also sees that, with the exception of HT-K_2AgF_4, the symmetries of the majority phases (as determined by zero or nonzero $B_{A\perp}^{int}$) of the mixed compounds are in agreement with the phase diagram of Figure 4.

One of the remaining puzzles concerns the form of the low-temperature HT-K_2AgF_4 spectra. Below 150 K, the spectrum is clearly rhombic whereas the one obtained for the $K_{1.5}Rb_{0.5}AgF_4$ compound (SI, Section VI) is not, even though it has an almost identical b/a ratio at this temperature. This may be due to differences in the tilting of $[AgF_6]^{4-}$ octahedra in the two compounds and/or the disordered nature of the JT elongation axes within the 2D layers of the HT-K_2AgF_4 compound that could result in regions of the sample that are quite distorted, with other regions more closely resembling the tetragonal AE phase.

More interesting is the behavior upon cooling further into the supposed LTLO phase. XRPD data suggest that the b/a ratio approaches 1.00 (to within the precision of the measurements) at the lowest temperatures, yet the HT-K_2AgF_4 FMR spectra become even more rhombic. The evolution of the FMR spectrum from 100 to 3 K reveals that the lowest-field (x-) component shifts appreciably to lower field and remains sharp/well-defined; the z component exhibits similar behavior, although shifting to higher field. In contrast, the intermediate (y) component seen at ∼10.5 T at 50 K essentially washes out (i.e., it spreads apart into a series of successively smaller peaks with decreasing temperature). However, one can just about see one remaining component at ∼10.5 T at the lowest temperature in Figures 7c and 8b. If one associates this with the y component of the spectrum, one then sees that the x and y resonances again split symmetrically about the axial position of the M = Cs compound. In other words, it appears that the axial saturation anisotropy field, $B_{A\parallel}^{int}$, is the same as in the other layered compounds whereas the perpendicular component (associated with at least part of the sample), $B_{A\perp}^{int}$, is about a factor of 3 stronger than found for the orthorhombic LTO phase (Table 4).

Very similar trends to those noted above can be seen in the inset to Figure 9a, which shows low-temperature, field-dependent spectra for HT-K_2AgF_4. A rhombic spectrum is seen at the lowest field/frequency, with clearly discernible x and y resonances, although their separation is considerably less than at high fields due to a reduction in the Zeeman interaction. Upon increasing the field, the y resonance again washes out in essentially the same way that it does for the high-field spectra upon cooling. This clearly indicates that the vanishing of the intermediate component of the spectrum is connected to the saturation of the ordered FM moment and the resulting perpendicular anisotropy field, $B_{A\perp}^{int}$ (and associated exchange interactions).

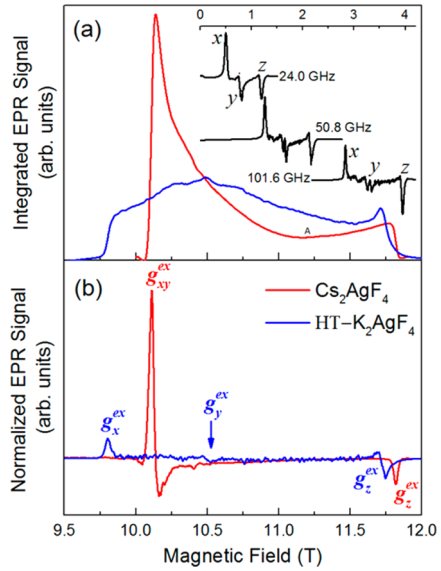

Figure 9. (Main panel) Comparison of 3 K, 326 GHz absorption spectra for (a) Cs_2AgF_4 and HT-K_2AgF_4 that were obtained through integration of the EPR spectra (b). The spectra have been normalized by comparing the 200 K paramagnetic spectra in order to correct for the total number of spins in each sample. The inset in panel a displays low-field EPR spectra of HT-K_2AgF_4 measured at 5 K and the indicated low microwave frequencies.

How this happens is seen most clearly in the main panels of Figure 9, which compare normalized 3 K spectra for the M = Cs and HT-K compounds in both absorption (a) and derivative (b) modes. The axial (and presumably well-ordered) Cs compound shows a strong onset of absorption at 10.1 T that is due to the perpendicular (xy) component of the g tensor. A much (9-fold) weaker onset is seen at 9.8 T for the biaxial AE_α^{disord} K compound and hence the much weaker $g^{ex}{}_x$ peak in Figure 9b, suggesting that a relatively small fraction of the sample experiences the maximal $B_{A\perp}^{int}$ field reported in Table 4. Note that this is not the case for the parallel (z) components. The maximum g value measured from the slope of the frequency dependence at the low-field end of the spectra is g_x^{ex} = 2.30 (Figure S2). Because g_{xy}^{ex} = 2.26 was observed at 200 K,

DOI: 10.1021/acs.inorgchem.6b02037
Inorg. Chem. 2016, 55, 11479−11489

the minimum g_y^{ex} value should be around 2.22, according to eqs 2a and 2b. The difference between g_{xy}^{ex} (200 K) and g_x^{ex} (3 K) also implies an ∼13° tilt from the perfect perpendicular arrangement in good agreement with a value of 16.2 deg derived from DFT+U calculations.[29] The disorder in the HT-K_2AgF_4 compound therefore causes a redistribution of the absorption intensity extending over much of the spectrum and hence the much flatter absorption profile and an essentially complete suppression of the intermediate $g^{ex}{}_y$ feature in the derivative spectrum. The fact that the parallel component does not appear to be affected confirms that the disorder is confined mainly to the *xy* plane. This could be due to a complete switching of the sign of the exchange (from FM to AFM) interaction between some near-neighbor Ag(II) sites with abnormally oriented (parallel) JT elongation axes. This would affect not only the local exchange anisotropy but also would give rise to spin frustration, resulting in a local suppression of spin correlations $\langle \hat{s}_i \cdot \hat{s}_j \rangle$. Disorder associated with the tilting of the $[AgF_6]^{4-}$ octahedra may also influence the local exchange anisotropies, although the effects of the abnormally oriented JT axes will likely have a much stronger influence.

More on Tilting Patterns. Because of the previously mentioned problems of discerning the type of JT order present in M_2AgF_4 by the powder X-ray diffraction method, we cannot conclude from those data what kind of ordering scenario is present in the LTLO, LTO, and HTT phases. Previous DFT + U calculations[29] show that FC-type phases are over 100 meV/fu higher in energy than the AE-type structures. Such an energy difference corresponds to temperatures above 1100 K and thus indicates that in the studied temperature range the $K_{2-x}Rb_xAgF_4$ phases should exhibit AE-type structures. Thus, the observed phase transitions should originate solely from differences in tilting distortions, possibly from the transition from α-type distortions to β-type ones. (The differences between these distortion types is discussed in ref 29.)

CONCLUSIONS AND OUTLOOK

We have studied the M_2AgF_4 series (M = K, $K_{3/4}Rb_{1/4}$, $K_{1/2}Rb_{1/2}$, $K_{1/4}Rb_{3/4}$, Rb, Cs) using temperature-resolved X-ray diffraction and heat capacity measurements, magnetometry, and HFEPR spectroscopy. Our results suggest that all double-perovskite fluoroargentates(II) phases, including HT-K_2AgF_4, adopt structures consisting of an antiferrodistortive arrangement of the elongated $[AgF_6]^{4-}$ octahedra, in agreement with recent theoretical calculations.[29] The HFEPR spectra show that the structures of the M = K, $K_{3/4}Rb_{1/4}$, $K_{1/2}Rb_{1/2}$, $K_{1/4}Rb_{3/4}$ members of the series are most complex, with local distortions and possibly even composition inhomogeneity, despite their seemingly single-phase character in powder X-ray diffraction.

The temperature-resolved phase diagram of the M = K/Rb phases has been investigated in the 2−350 K temperature window, adding to the existing data for the M = Na to Cs members. This phase diagram shows a systematic trend in the temperatures of the phase transitions involving two orthorhombic phases and one tetragonal phase, which most probably arises from various tilting distortions within the double-perovskite structure. The phase diagram is further complicated by the thermodynamic preference for the 1D postperovskite structure for M = Na, K.

The importance of the correct assignment of the JT order in Ag(II) fluorides lies in the strong dependence of the magnetic properties on the structure of these compounds. As calculations show, the AE distortion induces FM coupling within the $[AgF_{4/2+2}]^{2-}$ planes of the layered-perovskite phases and FC ordering would lead to antiferromagnetic (AFM) interactions.[29] The fact that M_2AgF_4 compounds adopt AE-type structures and hence are FM at low temperatures makes them dissimilar from La_2CuO_4. Therefore, the present study offers experimental evidence that the M_2AgF_4 systems are unlikely to constitute good precursors for HTSCs. Still, the connectivity of the Ag/F sublattice might be modified by the application of high pressure, by analogy to studies on K_2CuF_4.[41] The results of our high-pressure studies on M_2AgF_4 will be published shortly elsewhere.

ASSOCIATED CONTENT

Supporting Information

The Supporting Information is available free of charge on the ACS Publications website at DOI: 10.1021/acs.inorgchem.6b02037.

Room-temperature XRDP of Rb_2AgF_4; frequency dependence of the field components of the EPR spectra obtained for HT-K_2AgF_4; temperature-resolved XRDP measurements for $K_{2-x}Rb_xAgF_4$; heat capacity measurements for $K_{2-x}Rb_xAgF_4$; Raman measurements; HFEPR spectra of $K_{1.5}Rb_{0.5}AgF_4$ and $K_{0.5}Rb_{1.5}AgF_4$; XRDP diffractograms at 80 K; comparison between X-band and HFEPR spectra; photograph of a holder for conducting HFEPR measurements; and HT-K_2AgF_4 structure (AE_α^{disord}) in CIF format (PDF)

AUTHOR INFORMATION

Corresponding Authors

*E-mail: d.kurzydlowski@cent.uw.edu.pl.
*E-mail: ozarowsk@magnet.fsu.edu.
*E-mail: shill@magnet.fsu.edu.
*E-mail: zoran.mazej@ijs.si.
*E-mail: w.grochala@cent.uw.edu.pl.

Funding

We acknowledge support from the Polish National Science Centre (NCN) within the HARMONIA project "HP" (project 2012/06/M/ST5/00344). Z.M. gratefully acknowledges the Slovenian Research Agency (ARRS) for the financial support of the present study within research program P1-0045 Inorganic Chemistry and Technology. The high-field EPR spectra were recorded at the NHMFL, which is funded by the NSF through cooperative agreement no. DMR-1157490 and the State of Florida. S.H. thanks the NSF for financial support (grant DMR-1309463). Selected measurements were carried out by using the CEPT infrastructure financed by the EU European Regional Development Fund within the Operational Programme "Innovative Economy" for 2007−2013 (POIG.02.02.00-14-024/08-00).

Notes

The authors declare no competing financial interest.

ACKNOWLEDGMENTS

We are grateful to Dr. Evgeny Goreshnik (IJS, Ljubljana) for reexamining the earlier results of measurements for HT-K_2AgF_4 (SI). This work is dedicated to Prof. Tomasz Dietl on his 65th birthday.

REFERENCES

(1) Odenthal, R.-H.; Hoppe, R. Fluorargentate(II) der Alkalimetalle. *Monatsh. Chem.* **1971**, *102*, 1340−1350.

DOI: 10.1021/acs.inorgchem.6b02037
Inorg. Chem. 2016, 55, 11479−11489

(2) Odenthal, R.-H.; Hoppe, R. Z. Uber Fluoroargentate(II) $M^{II}[AgF_4]$ mit M^{II} = Ba, Sr, Ca, Hg, Cd, sowie Ba_2AgF_6. *Z. Anorg. Allg. Chem.* **1971**, *385*, 92−101.
(3) Odenthal, R.-H.; Paus, D.; Hoppe, R. Z. Zur Magnetochemie der Fluoroargentate(II): Messungen an $Ba[AgF_4]$, $Sr[AgF_4]$, Ba_2AgF_6 sowie $K[AgF_3]$ und $Cs[AgF_3]$. *Z. Anorg. Allg. Chem.* **1974**, *407*, 151−156.
(4) Odenthal, R.-H.; Paus, D.; Hoppe, R. Z. Zur Magnetochemie des zweiwertigen Silbers Neue Fluoroargentate(II): Cs_2AgF_4, Rb_2AgF_4 und K_2AgF_4. *Z. Anorg. Allg. Chem.* **1974**, *407*, 144−150.
(5) Grochala, W.; Hoffmann, R. Real and Hypothetical Intermediate-Valence Ag(II)/Ag(III) and Ag(II)/Ag(I) Fluoride Systems as Potential Superconductors. *Angew. Chem., Int. Ed.* **2001**, *40*, 2742−2781.
(6) Grochala, W. The theory-driven quest for a novel family of superconductors: fluorides. *J. Mater. Chem.* **2009**, *19*, 6949−6968.
(7) Norman, M. R. Materials design for new superconductors. *Rep. Prog. Phys.* **2016**, *79*, 074502.
(8) Grochala, W. Magnetism: Small changes, big consequences. *Nat. Mater.* **2006**, *5*, 513−514.
(9) Grochala, W.; Mazej, Z. Chemistry of silver (II): a cornucopia of peculiarities. Z. *Philos. Trans. R. Soc., A* **2015**, *373*, 20140179.
(10) Mazej, Z.; Kurzydłowski, D.; Grochala, W. Unique Silver(II) Fluorides: The Emerging Electronic and Magnetic Materials. In *Photonic and Electronic Properties of Fluoride Materials*; Tressaud, A., Poeppelmeier, K., Eds.; Elsevier: Amsterdam, 2016; pp 231−260.
(11) Kurzydłowski, D.; Mazej, Z.; Jagličić, Z.; Filinchuk, Y.; Grochala, W. Structural transition and unusually strong antiferromagnetic superexchange coupling in perovskite $KAgF_3$. *Chem. Commun.* **2013**, *49*, 6262−6264.
(12) Radaelli, P.; Hinks, D.; Mitchell, A.; Hunter, B.; Wagner, J.; Dabrowski, B.; Vandervoort, K.; Viswanathan, H.; Jorgensen, J. Structural and superconducting properties of $La_{2-x}Sr_xCuO_4$ as a function of Sr content. *Phys. Rev. B: Condens. Matter Mater. Phys.* **1994**, *49*, 4163−4175.
(13) Vaknin, D.; Sinha, S.; Moncton, D.; Johnston, D. C.; Newsam, J.; Safinya, C.; King, H. Antiferromagnetism in La_2CuO_{4-y}. *Phys. Rev. Lett.* **1987**, *58*, 2802−2805.
(14) McLain, S. E.; Dolgos, M. R.; Tennant, D. A.; Turner, J. F. C.; Barnes, T.; Proffen, T.; Sales, B. C.; Bewley, R. I. Magnetic behaviour of layered Ag(II) fluorides. *Nat. Mater.* **2006**, *5*, 561−565.
(15) Reinen, D.; Friebel, C. Local and Cooperative Jahn-Teller Interactions in Model Structures Spectroscopic and Structural Evidence. *Struct. Bonding (Berlin, Ger.)* **1979**, *37*, 1−60.
(16) Falvello, L. R. Jahn−Teller effects in solid-state co-ordination chemistry. *J. Chem. Soc., Dalton Trans.* **1997**, 4463−4476.
(17) Lancaster, T.; Blundell, S.; Baker, P.; Hayes, W.; Giblin, S.; McLain, S. E.; Pratt, F.; Salman, Z.; Jacobs, E.; Turner, J.; Barnes, T. Intrinsic magnetic order in Cs_2AgF_4 detected by muon-spin relaxation. *Phys. Rev. B: Condens. Matter Mater. Phys.* **2007**, *75*, 220408.
(18) Tong, J.; Kremer, R. K.; Köhler, J.; Simon, A.; Lee, C.; Kan, E.; Whangbo, M.-H. The layered ferromagnet Cs_2AgF_4: Antiferromagnetic inter-layer coupling driven by magnetic dipole-dipole interactions. *Zeitschrift für Krist.* **2010**, *225*, 498−503.
(19) Mazej, Z.; Goreshnik, E.; Jagličić, Z.; Gaweł, B.; Łasocha, W.; Grzybowska, D.; Jaroń, T.; Kurzydłowski, D.; Malinowski, P. J.; Koźmiński, W.; Szydłowska, J.; Leszczyński, P. J.; Grochala, W. $KAgF_3$, K_2AgF_4 and $K_3Ag_2F_7$: important steps towards a layered antiferromagnetic fluoroargentate(II). *CrystEngComm* **2009**, *11*, 1702−1710.
(20) Kurzydłowski, D.; Derzsi, M.; Budzianowski, A.; Jagličić, Z.; Koźmiński, W.; Mazej, Z.; Grochala, W. Polymorphism of Fluoroargentates(II): Facile Collapse of a Layered Network of α-K_2AgF_4 Due to the Insufficient Size of the Potassium Cation. *Eur. J. Inorg. Chem.* **2010**, *2010*, 2919−2925.
(21) Kurzydłowski, D.; Mazej, Z.; Grochala, W. Na2AgF4:1D antiferromagnet with unusually short $Ag^{2+}\cdots Ag^{2+}$ separation. *Dalton Trans* **2013**, *42*, 2167−2173.
(22) Tong, J.; Köhler, J.; Simon, A.; Lee, C.; Whangbo, M.-H. Optical properties of the orchid colored silver(II) Fluoride Cs_2AgF_4. *Z. Anorg. Allg. Chem.* **2012**, *638*, 1792−1795.
(23) Friebel, C.; Reinen, D. Ligandenfeld- und ESR-spektroskopische Untersuchungen zum Jahn-Teller-Effekt des Ag^{2+}-Ions in fluoridischer Koordination. *Z. Anorg. Allg. Chem.* **1975**, *413*, 51−60.
(24) Kasinathan, D.; Koepernik, K.; Nitzsche, U.; Rosner, H. Ferromagnetism Induced by Orbital Order in the Charge-Transfer Insulator Cs_2AgF_4: An Electronic Structure Study. *Phys. Rev. Lett.* **2007**, *99*, 247210.
(25) Wu, H.; Khomskii, D. I. Orbital ordering in the ferromagnetic insulator Cs_2AgF_4 from first principles. *Phys. Rev. B: Condens. Matter Mater. Phys.* **2007**, *76*, 155115.
(26) Liu, D.-Y.; Lu, F.; Zou, L.-J. Anharmonic effect on lattice distortion, orbital ordering and magnetic properties in Cs_2AgF_4. *J. Phys.: Condens. Matter* **2009**, *21*, 026014.
(27) Zhang, X.; Zhang, G.; Jia, T.; Zeng, Z.; Lin, H. Q. α-K_2AgF_4: Ferromagnetism induced by the weak superexchange of different e_g orbitals from the nearest neighbor Ag ions. *AIP Adv.* **2016**, *6*, 055702.
(28) Jaroń, T.; Grochala, W. Prediction of giant antiferromagnetic coupling in exotic fluorides of Ag^{II}. *Phys. Status Solidi RRL* **2008**, *2*, 71−73.
(29) Kurzydłowski, D.; Derzsi, M.; Mazej, Z.; Grochala, W. Crystal, electronic, and magnetic structures of M_2AgF_4 (M = Na−Cs) phases as viewed from the DFT+U method. *Dalton Trans.*, in press **2016**. DOI: 10.1039/C6DT03125K.
(30) Petricek, V.; Dusek, M.; Palatinus, L. Jana2006. *The Crystallographic Computing System*; Institue of Physics: Praha, 2006.
(31) Hammersley, A. P.; Svensson, S. O.; Hanfland, M.; Fitch, A. N.; Hausermann, D. Two-dimensional detector software: From real detector to idealised image or two-theta scan. *High Pressure Res.* **1996**, *14*, 235−248.
(32) Rodríguez-Carvajal, J. Recent advances in magnetic structure determination by neutron powder diffraction. *Phys. B* **1993**, *192*, 55−69.
(33) Hassan, A.; Pardi, L.; Krzystek, J.; Sienkiewicz, A.; Goy, P.; Rohrer, M.; Brunel, L.-C. Ultrawide Band Multifrequency High-Field EMR Technique: A Methodology for Increasing Spectroscopic Information. *J. Magn. Reson.* **2000**, *142*, 300−312.
(34) Bain, G. A.; Berry, J. F. Diamagnetic Corrections and Pascal's Constants. *J. Chem. Educ.* **2008**, *85*, 532−536.
(35) Reinen, D.; Krause, S. Local and cooperative Jahn-Teller interactions of copper(2+) in host lattices with tetragonally compressed octahedra. Spectroscopic and structural investigation of the mixed crystals $K(Rb)_2Zn_{1-x}Cu_xF_4$. *Inorg. Chem.* **1981**, *20*, 2750−2759.
(36) Baker, G. A.; Gilbert, H. E.; Eve, J.; Rushbrooke, G. S. On the two-dimensional, spin- Heisenberg ferromagnetic models. *Phys. Lett. A* **1967**, *25*, 207−209.
(37) Winter, S. M.; Datta, S.; Hill, S.; Oakley, R. T. Magnetic anisotropy in a heavy atom radical ferromagnet. *J. Am. Chem. Soc.* **2011**, *133*, 8126−8129.
(38) Abragam, A.; Bleaney, B. Electron Paramagnetic Resonance of Transition Ions; Oxford University Press: Oxford, 2012.
(39) Winter, S. M.; Hill, S.; Oakley, R. T. Magnetic Ordering and Anisotropy in Heavy Atom Radicals. *J. Am. Chem. Soc.* **2015**, *137*, 3720−3730.
(40) Winter, S. M.; Oakley, R. T.; Kovalev, A. E.; Hill, S. Spin-orbit effects in heavy-atom organic radical ferromagnets. *Phys. Rev. B: Condens. Matter Mater. Phys.* **2012**, *85*, 094430.
(41) Ishizuka, M.; Terai, M.; Hidaka, M.; Endo, S.; Yamada, I.; Shimomura, O. Pressure-induced structural phase transition in the two-dimensional Heisenberg ferromagnet K_2CuF_4. *Phys. Rev. B: Condens. Matter Mater. Phys.* **1998**, *57*, 64−67.

DOI: 10.1021/acs.inorgchem.6b02037
Inorg. Chem. 2016, 55, 11479−11489